





26 and observed marked improvements after calibration and regionalization. We also  
27 generated gridded parameter sets for both models across all 4816 HUC-10 basins in  
28 the Western U.S., a data set that is intended to support regional hydrologic studies and  
29 hydrologic climate change assessments.

## 30 **1. Introduction**

31 Streamflow forecasts play a key role in various aspects of water and  
32 environmental management, especially in the Western U.S. (WUS). In the short term,  
33 these forecasts provide early warnings for impending flood events, thereby enabling  
34 timely preparation and response to mitigate immediate flood risk and damages  
35 (Maidment, 2017). They also serve as crucial input for managing reservoirs  
36 effectively for water supply (Raff et al., 2013), hydroelectric power generation  
37 (Boucher & Ramos, 2018), and river navigation (by providing a basis for predicting  
38 water levels) (Federal Institute of Hydrology, 2020). In the longer term, streamflow  
39 forecasts enable water utilities and agencies to plan water distribution within and  
40 across multiple uses—urban, agricultural, and industrial—which is especially vital  
41 during drought conditions when efficient water use becomes a necessity (Anghileri et  
42 al., 2016;). Streamflow forecasts also aid in understanding and predicting the impacts  
43 of climate change on water systems, thereby informing adaptive strategies for water  
44 resource management. Thus, in both short and longer-term contexts, streamflow  
45 forecasts are an important tool for promoting sustainable water practices and  
46 resilience to water-related challenges.

47 Streamflow forecasts are derived via a synthesis of hydrometeorological data,  
48 statistical methodologies, and computational modeling. Direct measurement of runoff  
49 is an important element of streamflow forecasts, however it is only possible in river  
50 basins with well-developed observational infrastructure (Sharma and Machiwal,



51 2021). This limitation leaves vast areas, often critical to water resource management  
52 and climatology, without direct runoff observations on which to base streamflow  
53 forecasts. As an alternative, Land Surface Models (LSMs) can be used to simulate  
54 streamflow. LSMs typically are forced with air temperature, precipitation and other  
55 meteorological forcings. By integrating climatic, topographic, and land-use  
56 information, they can fill streamflow observation gaps and provide comprehensive,  
57 spatially distributed runoff forecasts (Fisher and Koven, 2020). The capabilities of  
58 LSMs equip us with the necessary tools to produce streamflow forecasts that can be  
59 used to prepare for severe weather conditions, form the basis for water resource  
60 management, and inform water management associated with our evolving climate.  
61 These benefits hold true irrespective of the limitations associated with direct  
62 streamflow observations. Through off-line simulations and reconstructions, LSMs  
63 enable us to gain insights into land surface hydrology at various scales - regional,  
64 continental, and global.

65 The parameterization of the underlying hydrological processes varies across  
66 different LSMs, but virtually all models require some level of parameter estimation  
67 based on historical observed streamflow data at forecast point, to ensure trustworthy  
68 predictions throughout the region (Beven, 1989; Troy et al., 2008; Gong et al., 2015).  
69 In cases where observations don't exist, parameters can be transferred from river  
70 basins where they do (Arsenault and Brissette (2014)). In cases where observations  
71 do exist but aren't current, we can use a shorter span of historical streamflow data for  
72 model calibration and subsequently produce streamflow forecasts using  
73 meteorological forcings when observed streamflow data aren't available.

74 The process of calibration can be computationally demanding, and prior research  
75 typically has focused on obtaining parameters appropriate to facilitating model  
76 simulations that match observations as closely as possible at the observation point



77 (Duan et al,1992; Tolson and Shoemaker, 2007). Most previous studies have  
78 concentrated on a limited number of basins and a single model (e.g. Mascaro et al.,  
79 2023; Sofokleous et al., 2023; and Gou et al., 2020). Here, we aim to establish  
80 parameterizations for two LSMs -- the Variable Infiltration Capacity (VIC) model and  
81 the Noah-Multiparameterization (Noah-MP) LSM across the WUS. Both models  
82 have found extensive application both within the U.S. and internationally (Mendoza et  
83 al.,2015; Tangdamrongsub, 2023). The approach we use involves the application of  
84 globally optimized calibration methods and regionalization, with the objective of  
85 facilitating these models to provide reliable runoff simulations.

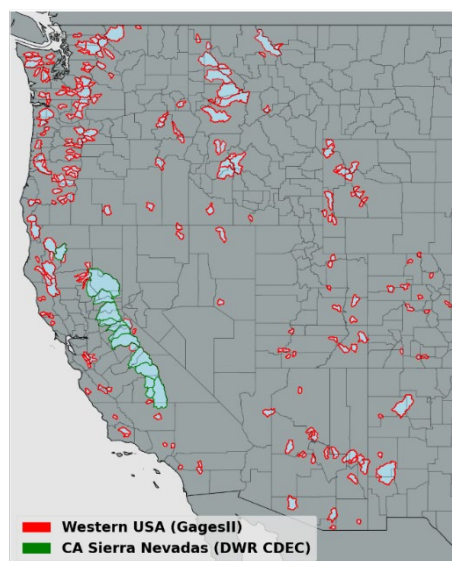
86 In particular, we explore and elucidate (i) the choice of physical  
87 parameterizations and calibration of land surface parameters, (ii) extension of these  
88 calibrated parameters to areas without gauges, and (iii) factors that influence  
89 calibration efficiency and LSM performance using regional parameter estimates. In  
90 the case of Noah-MP, which offers multiple runoff generation (physics) options, our  
91 initial step involves choosing the most effective runoff parameterization option.  
92 Following this, we perform the calibration of land surface parameters. In the case of  
93 the VIC model, the runoff parameterization scheme is predetermined, so we  
94 commence immediately with calibration. We implemented calibration in 263 basins  
95 across the WUS where streamflow observations were available (see section 2.1 for  
96 details) and compared simulated and observed streamflow as the model predictions  
97 were affected by soil and other land surface properties. Our second step extended the  
98 initial calibrated land surface parameters to ungauged basins. We then explored the  
99 variables that most impact the calibration proficiency of Noah-MP and VIC across the  
100 WUS. In section 4, we employ a regionalization technique known as the donor basin  
101 method, as implemented by Bass et al. (2023). Finally, we evaluate both flood and  
102 low flow simulation skills for the baseline, and after calibration and regionalization.



103        **2. Study basins, land surface models and forcing dataset overview**

104        **2.1 Study Basins**

105        We selected 263 river basins distributed across the WUS. Most of the basins  
106        were from USGS Gages II reference basins (Falcone 2011) which have minimum  
107        upstream anthropogenic effects such as dams and diversions. Among these basins,  
108        our selection criteria included having at least 20 years of record, and a minimum  
109        drainage area of 144 square kilometers, which is the size of four model grid cells. In  
110        addition to 250 Gages II reference stations, we included 13 basins located in  
111        California's Sierra Nevada for which natural flows are available from the California  
112        Department of Water Resources (2021). The geographical distribution of the 263  
113        basins is shown in Figure 1. We focused on the hydrological models' calibration to  
114        full natural flow (the same as observed streamflow for GAGES II stations; estimated  
115        by DWR for the 13 Sierra Nevada sites), which indicates water flow conditions  
116        devoid of human interventions like reservoirs or diversions. Each basin was calibrated  
117        using the most recent 20-year period when the observation is available.



118

119           Figure. 1. 263 river basins for which calibration was performed. The Gages II  
120 reference basins are delineated with red boundaries and the CA Sierra Nevada basins  
121 with green boundaries.

## 122           2.2 Land Surface Models

123           We included two widely used hydrological models, VIC (Liang et al., 1994) and  
124 Noah-MP (Niu et al. 2011). This decision was informed by the varying levels of  
125 complexity these two models offer in conceptualizing the effects of vegetation, soil,  
126 and seasonal snowpack on the land surface energy and water balances (refer to Table  
127 1 for more details). The two models also use different parameterizations for certain  
128 hydrological processes, including unique model equations for canopy water storage,  
129 base flow, and other processes. Both of these hydrological model structures have  
130 found extensive application both within the U.S. and internationally, as indicated by  
131 Mendoza et al. (2015) and Tangdamrongsub (2023).

132           To generate streamflow, the gridded runoff from Noah-MP and VIC was



133 accumulated over each watershed. We didn't implement routing since its impact on  
134 daily streamflow simulations was small given the relatively small size of most of the  
135 basins. This aligns with earlier research (e.g., Li et al. 2019). However, in both the  
136 case of VIC and Noah-MP, the output of our simulations (runoff) could be used as  
137 input to routing models, such as those that are options in the implementation of both  
138 models.

### 139 **2.2.1 VIC**

140 VIC is a macroscale, semi-distributed hydrologic model (described in detail by  
141 Liang et al 1994) that determines land surface moisture and energy states and fluxes  
142 by solving the surface water and energy balances. VIC is a research model and in its  
143 various forms it has been employed to study many major river basins worldwide (e.g.  
144 Adam et al 2003 & 2006; Livneh et al 2013; Schaperow et al 2021). This model  
145 enjoys a broad user community — as per the citation index Web of Science, the initial  
146 VIC paper has been referenced more than 2600 times, with contributing authors  
147 spanning at least 56 different countries (Schaperow et al 2021). We obtained initial  
148 VIC model parameters from Livneh et al 2013, who validated model discharges over  
149 major CONUS river basins. The origins of the soil and land cover data are outlined in  
150 Table 1. The version of the VIC model implemented here is 4.1.2, and it operates in  
151 energy balance mode.

### 152 **2.2.2 Noah-MP**

153 Noah-MP is a state-of-the-art LSM originally designed as the land surface  
154 scheme for numerical weather prediction (NWP) models like the Weather Research  
155 and Forecasting (WRF) regional atmospheric model. Currently, it's being utilized for  
156 physically based, spatially-distributed hydrological simulations as a component of the



157 National Water Model (NWM) (NOAA, 2016). It enhances the functionalities of the  
158 Noah LSM (as per Chen et al., 1996 and Chen and Dudhia, 2001) previously used in  
159 NOAA's suite of numerical weather prediction models by offering multiple options  
160 for key processes that control land-atmosphere transfers of moisture and energy.  
161 These include surface water infiltration, runoff, evapotranspiration, groundwater  
162 movement, and channel routing (see Niu et al., 2007; 2011). The model has been  
163 widely used for forecasting seasonal climate, weather, droughts, and floods not only  
164 across the continental United States (CONUS) but also globally (Zheng et al., 2019).

### 165 **2.3 Forcing Dataset**

166 We ran both models at a 3-hour time step and at  $1/16^\circ$  latitude–longitude spatial  
167 resolution. The forcings were the gridded observation dataset developed by Livneh et  
168 al (2013) and extended to 2018 by Su et al (2021) (hereafter referred to as L13). This  
169 data set spans the period from 1915 to 2018. For the VIC model, the L13 dataset  
170 provided daily values of precipitation, maximum and minimum temperatures, and  
171 wind speed (additional variables used by VIC including downward solar and  
172 longwave radiation, and specific humidity, are computed internally using MTCLIM  
173 algorithms as described by Bohn et al. (2013)). The Noah-MP model, on the other  
174 hand, necessitated additional meteorological data such as specific humidity, surface  
175 pressure, and downward solar and longwave radiation, in addition to precipitation,  
176 wind speed, and air temperature. We used the MTCLIM algorithms, as detailed by  
177 Bohn et al. (2013), to calculate specific humidity and downward solar radiation. We  
178 employed the Prata (1996) algorithm to compute the downward longwave radiation.  
179 Additionally, we deduced surface air pressure by considering the grid cell elevation in  
180 conjunction with standard global pressure lapse rates. Following this, we transitioned  
181 the daily data to hourly metrics using a cubic spline to interpolate between Tmax and





182 Tmin, and derived other variables using the methods explained by Bohn et al. (2013).

183 Lastly, we distributed the daily precipitation evenly across three hourly intervals.

184 Table 1. Overview of hydrologic model components and parameter data sources.

MODE L	SNOW ACCUMULATION AND MELT	MOISTURE IN THE SOIL AND COLUMN/SURFACE RUNOFF	BASE FLOW	CANOPY STORAGE	VEGETATION DATA	SOIL DATA
VIC (V4.1.2)	Two-layer energy–mass balance model	Infiltration capacity function. Vertical movement of moisture through soil follows 1D Richards equation.	A function of the soil moisture in the third layer. Linear below a soil moisture threshold and becomes nonlinear above that threshold. [Liang et al., 1994]	Mosaic representation of different vegetation coverages at each cell.	University of Maryland 1-km Global Land Cover Classification (Hansen et al. 2000)	1-km STAT SGO database (Miller and White 1998).
NOAH-MP (WRF-HYDRO 5.2.0)	Three-layer energy–mass balance model that represents percolation, retention, and refreezing of meltwater within the snowpack.	1. TOPMODEL-based runoff scheme	Simple groundwater (hereafter SIMGM) [Niu et al., 2007].	Semi-tile approach for computing longwave, latent heat, sensible heat and ground heat fluxes	MODIS 30-second Modified IGBP 20-category land cover product	1-km STAT SGO database (Miller and White 1998).
		2. Simple TOPMODEL-based runoff scheme with an equilibrium water table (hereafter SIMTOP)	Similar to SIMGM, but with a sealed bottom of the soil column [Niu et al., 2005]			
		3. Infiltration-excess-based surface runoff scheme	Gravitational free-drainage subsurface runoff scheme [Schaake et al., 1996]			
		4. BATS runoff scheme, which parameterized surface runoff as a 4th power function of the top 2 m soil wetness (degree of saturation)	Gravitational free drainage [Dickinson et al., 1993]			

185 **3. Model calibration**

186 **3.1 Calibration methods**

187 The initial step in our calibration effort was to optimize the land surface  
 188 parameters of the two models for the 253 WUS basins. These parameters, primarily  
 189 soil properties which can exhibit a substantial degree of uncertainty, were iteratively  
 190 updated via hundreds of simulations to accurately reflect streamflow conditions in  
 191 each basin. We calibrated six parameters for VIC and five for Noah-MP. This



192 selection was guided by past research and the computational resources we had at our  
193 disposal (Mendoza et al. 2015; Hussein 2020; Shi et al. 2008; Holtzman et al., 2020;  
194 Bass et al., 2023; Schaperow et al., 2023). Each parameter underwent consideration  
195 across a physically viable range (refer to Table 2), drawing from values utilized in  
196 prior studies (Cai et al. 2014; Mendoza et al. 2015; Hussein 2020; Shi et al. 2008;  
197 Gochis et al., 2019; Holtzman et al., 2020; Lahmers et al. 2021; Bass et al., 2023;  
198 Schaperow et al., 2023). Through our iterative calibration method, each subsequent  
199 simulation learns from the previous ones using algorithms designed to reduce the  
200 discrepancy between the simulated and observed streamflow.

201 For VIC parameter estimation, we employed the Shuffled Complex Evolution  
202 algorithm developed at the University of Arizona (SCE-UA, Duan et al. 1992). This  
203 method is a global optimization method widely used in hydrology and environmental  
204 modeling, owing to its robustness and efficiency when addressing complex, non-  
205 linear, and multi-modal objective functions (Naeini et al., 2015).

206 For the Noah-MP model, which requires more computational core-hours per  
207 simulation, we used the Dynamically Dimensioned Search (DDS) algorithm of Tolson  
208 and Shoemaker (2007). This algorithm, specifically crafted for high-dimensional and  
209 computationally intensive problems, offers generally greater efficiency than SCE-UA.  
210 NOAA employs the DDS algorithm for their CONUS implementation of NWM,  
211 which is grounded in Noah-MP (Gochis et al. 2019). We evaluated both calibration  
212 methods (DDS and SCE-UA) for VIC for 20 randomly chosen basins, and obtained  
213 similar results. For VIC, we chose SCE-UA due to its inherent compatibility with the  
214 model and because the additional computation (relative to DDS) was less important  
215 given that the inherent computation required for VIC is considerably less than for  
216 Noah-MP.

217 In our application of SCE-UA, we performed a maximum of 3000 iterations for



218 each basin, while the DDS method employed 250 iterations for each basin for Noah-  
 219 MP. Each basin was calibrated using the most recent 20 years of streamflow data. For  
 220 both models, our objective function was the Kling-Gupta Efficiency (KGE, Gupta et  
 221 al., 2009) metric for daily streamflow. KGE is a widely used performance measure  
 222 because of its advantages in orthogonally considering bias, correlation and variability  
 223 (Knoben et al., 2019).  $KGE = 1$  indicates perfect agreement between simulations and  
 224 observations; KGE values greater than -0.41 indicate that a model improves upon the  
 225 mean flow benchmark (Konben et al., 2019).

226 TABLE 2. Calibration methods, parameters and modifications to their initial  
 227 default values evaluated in the calibration.

Model	VIC		Noah-MP	
Calibration Method	SCE-UA		DDS	
Iterations	3000		250	
Calibrated Parameter	Variable Infiltration Curve Parameter (INFILT)	0.001 – 0.4 (Shi et al.,2008)	Saturated Hydraulic Conductivity (Ksat)	$2 \times 10^{-9}$ to 0.07 (Cai et al.,2014)
	Baseflow parameter (Ds)	0.001 – 1.0 (Shi et al.,2008)	Saturation soil moisture content (MAXSMC)	0.1 to 0.71 (Cai et al.,2014)
	Thickness of Soil in Layer 1 (Depth_1)	0.01 – 0.2 (Shi et al.,2008)	Pore size distribution index (Bexp)	1.12 to 22 (Cai et al.,2014; Gochis et al.,2019)
	Total thickness of soil column (Depth_total)	0.6 – 3.5 (Shi et al.,2008)	Linear scaling of “openness” of bottom drainage boundary (Slope)	0.1-1 (Lahmers et al 2021)
	Max velocity parameter of baseflow (Dsmax)	0.001 – 30 (Schaperow et al.,2023)	Parameter in surface runoff (REFKDT)	0.1-10 (Lahmers et al 2021)
	Fraction of	0.001 – 1		



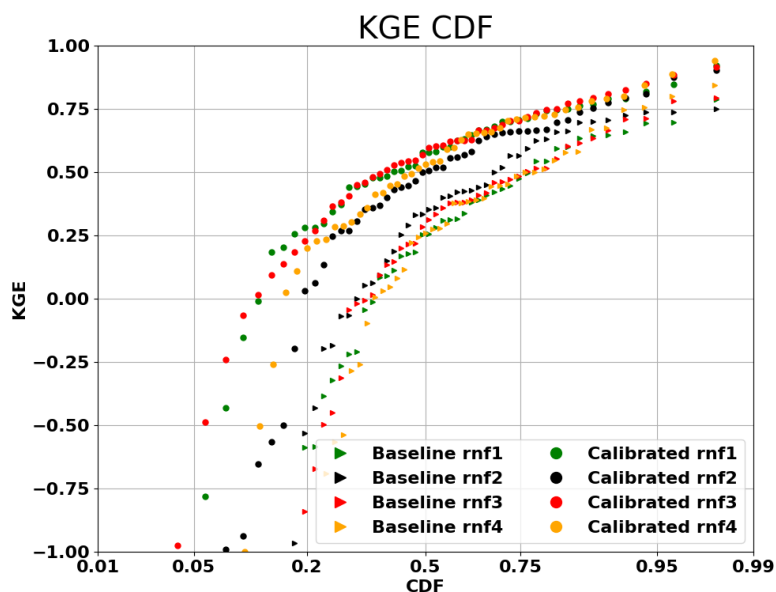
---

	max soil moisture where nonlinear baseflow occurs (Ws)	(Shi et al.,2008)
--	--	----------------------

---

228           **3.2 Noah-MP parameterization**

229           As specified in Table 1, Noah-MP has four runoff and groundwater physics  
230 options (rnf). Initially, we adopted the options that are incorporated in the NWM, as  
231 elaborated in Gochis et al. (2020). Before we could proceed with calibrating Noah-  
232 MP for all the WUS basins, it was necessary to determine suitable rnfs. To streamline  
233 computational time, we initially selected 50 basins randomly from the total of 263  
234 from which we created four experimental groups. Each group employed a different  
235 rnf option. We applied the DDS method to these groups and compared the cumulative  
236 distribution functions (CDF) of their baseline and calibrated KGEs (Figure 2). From  
237 this figure, it's apparent that the KGE improved post-calibration for all four rnfs.  
238 Notably, rnf3, also known as free drainage, exhibited the most substantial  
239 performance enhancement after calibration. As a result, we chose to continue using  
240 this option which is incorporated in the NWM. Nonetheless, it's worth noting that the  
241 use of different options for different basins—a feature currently not utilized in Noah-  
242 MP or WRF-Hydro—could potentially result in improved overall model performance.



243

244 Figure 2. Streamflow performance (KGE of daily streamflow simulations) of  
245 different Noah-MP runoff generation options across 50 (of 263) randomly selected  
246 basins. The performances are shown for both baseline and calibrated simulations.

### 247 3.3 Calibration of gauged basins

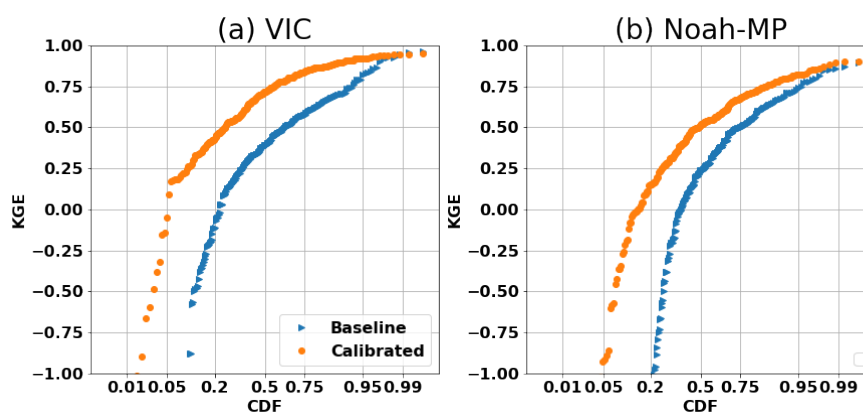
248 Following the selection of the most effective set of runoff generation options  
249 across the domain, we estimated model parameters for all 263 basins. The  
250 comparative performance of the models, before and after calibration, is shown in  
251 Figure 3. It's apparent from the figure that both Noah-MP and VIC have significantly  
252 enhanced their daily streamflow simulation skills post-calibration. After calibration,  
253 the median KGE of Noah-MP improved from 0.22 to 0.54, and the VIC's median  
254 KGE increased from 0.37 to 0.70. When contrasting the two models, we observed that  
255 VIC outperformed Noah-MP both pre- and post-calibration. One possible explanation  
256 could be that the baseline VIC parameters were taken from Livneh et al. (2013), and  
257 these parameters had already been validated and adjusted for major U.S. basins



258 (although not for our 263 basins specifically), while the Noah-MP parameters are  
259 default values from NWM. Another possibility is inherent differences in the physics  
260 of streamflow simulation between the two models (VIC primarily generates runoff via  
261 the saturation excess mechanism), although that isn't the main focus of our research.

262 Following the calibration with data from the past 20 years, we performed a test  
263 where we calibrated the streamflow using the first 10 years of data and validated with  
264 the subsequent 10 years of data. This test revealed that the KGE distribution from the  
265 10-year calibration is similar to that from the 20-year data. The median KGE values  
266 for VIC and Noah-MP after calibration with 10 years of observations were 0.52 and  
267 0.69, respectively. Correspondingly, the median KGEs during the validation period  
268 were 0.50 and 0.68, respectively, which are only slightly lower. These comparisons  
269 demonstrate general consistency over time in the performance of the calibrated  
270 parameters.

271



272

273 Figure 3. Cumulative Distribution Function (CDF) plot of the daily streamflow  
274 KGE for (a) VIC and (b) Noah-MP, comparing baseline and calibrated runs across all  
275 263 basins.



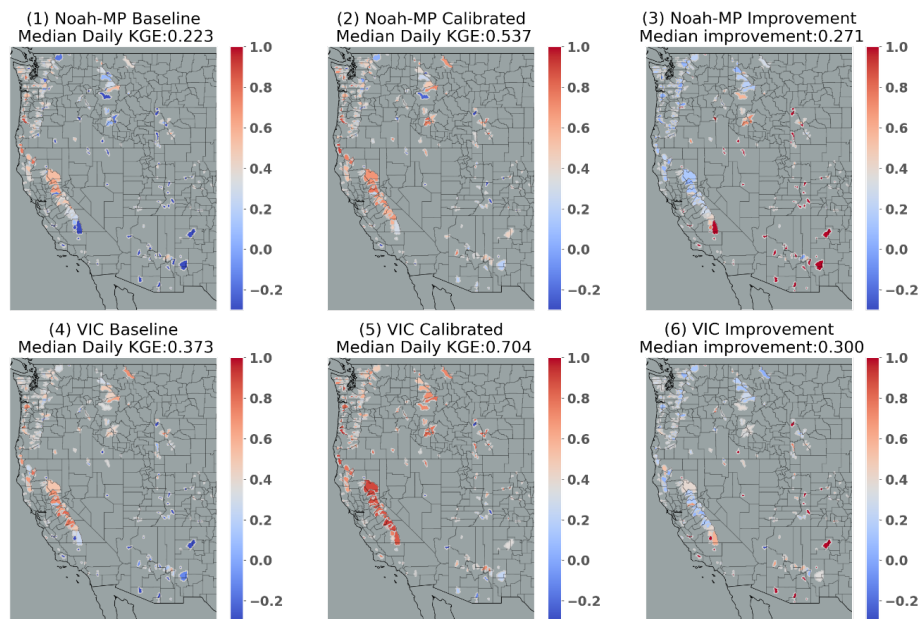
276 We examined the spatial variability of daily streamflow KGE for Noah-MP and  
277 VIC, both before and after the calibration (see Figure 4). The highest baseline KGEs  
278 are along the Pacific Coast, in central to northern CA for both models. VIC's baseline  
279 KGE generally is high in the Pacific Northwest. Post-calibration improvements  
280 occurred for both models in most areas, especially in regions where the baseline KGE  
281 was low, such as southern CA and the southeastern part of the study region. Median  
282 improvements after calibration were 0.27 for Noah-MP and 0.30 for VIC.

283 We observed that basins displaying higher KGE values typically were more  
284 humid than those with lower KGE. To further delve into the relationship between  
285 KGE and basin characteristics, we explored correlations between KGE and 21  
286 different characteristics, including drainage area, elevation, seasonal/annual average  
287 temperature and precipitation, annual maximum precipitation, and seasonal/annual  
288 runoff ratio. Of these, 12 characteristics were statistically significantly correlated with  
289 the VIC KGE, including four seasonal and annual runoff ratios; mean precipitation in  
290 winter, spring, and fall; annual maximum precipitation; and minimum elevation.  
291 Figure 5 shows scatterplots of eight representative characteristics. Apart from  
292 minimum elevation and mean summer temperature, all other characteristics were  
293 positively correlated with KGE. Typically, spring runoff ratio, annual runoff ratio,  
294 mean annual max precipitation, and mean winter precipitation exhibited the highest  
295 correlations with KGE. This implies that basins with higher runoff ratios (particularly  
296 in spring), higher precipitation (especially maximum precipitation), lower summer  
297 temperature, and lower elevation are more likely to exhibit strong VIC performance.  
298 The same applies to Noah-MP, as indicated in Figure 6, although Noah-MP showed  
299 relatively weaker correlations. Correlations between mean summer temperature and  
300 mean fall precipitation and Noah-MP KGE weren't statistically significant.

301 The spatial distribution of the eight characteristics is qualitatively similar with

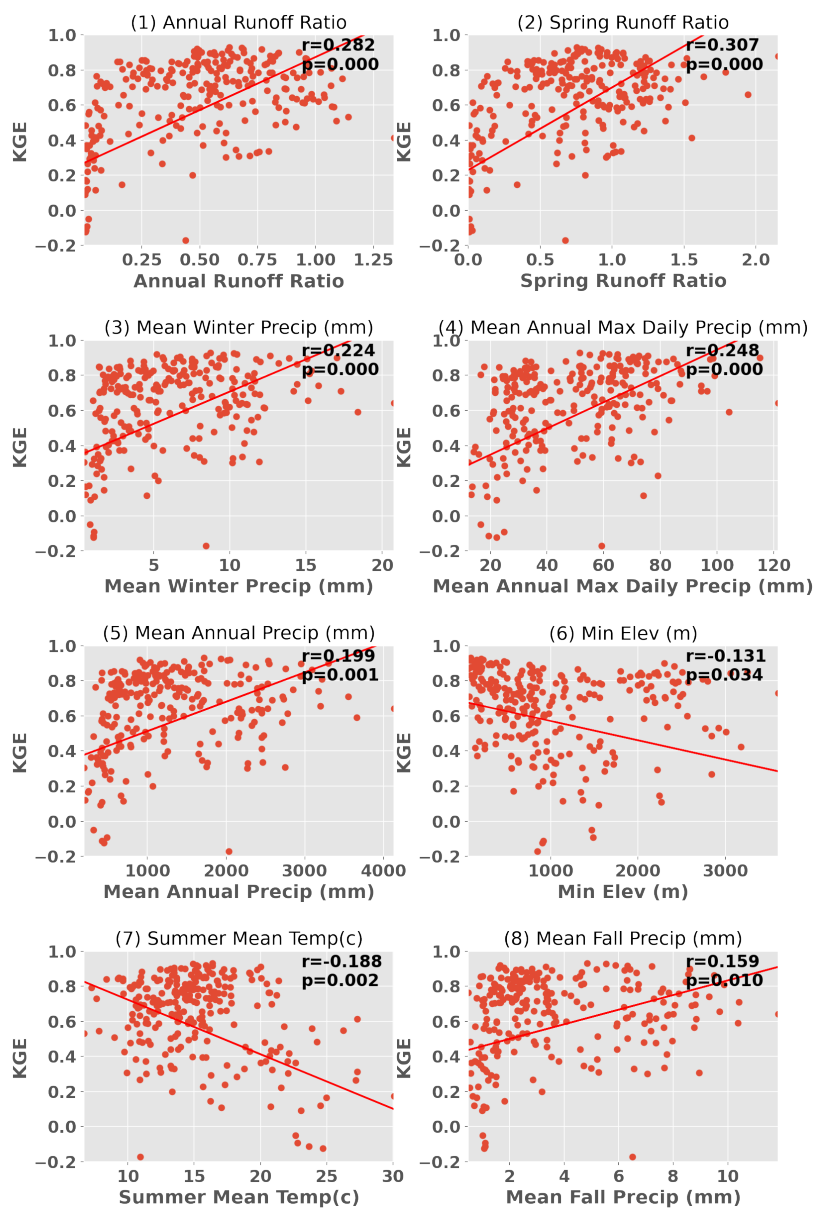


302 the KGE spatial distribution, as shown in Figure 7. Generally, basins with higher KGE  
303 have higher characteristic values when the correlation is positive, and lower  
304 characteristic values when the correlation is negative.



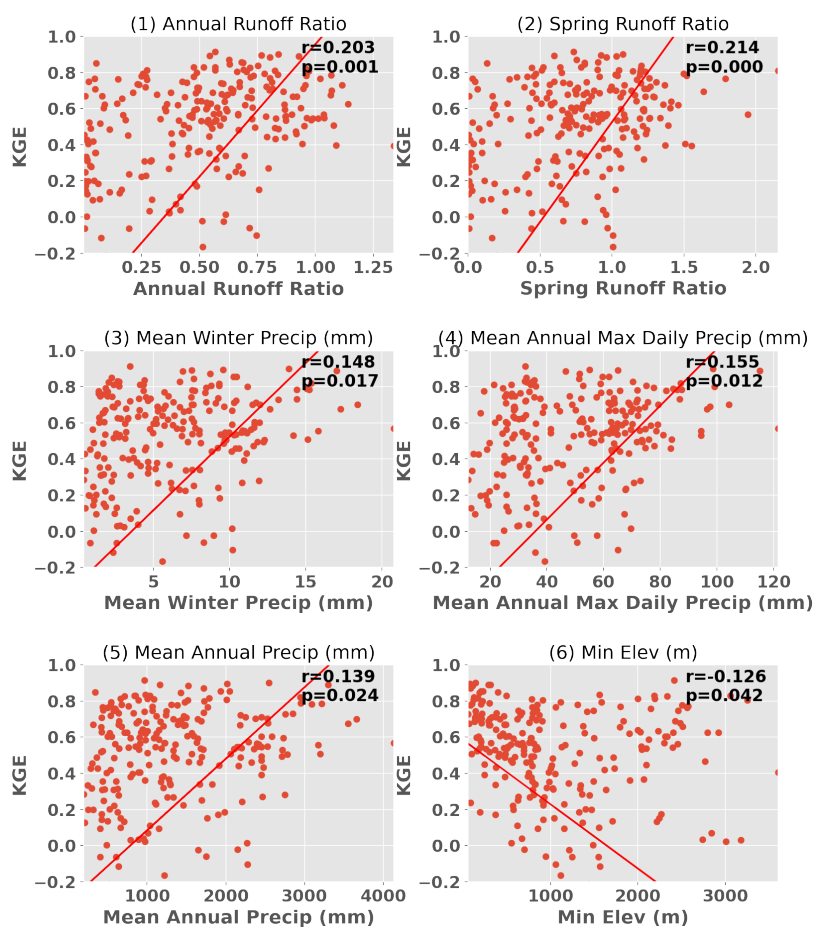
305  
306 Figure 4. Spatial distribution of daily streamflow KGE for Noah-MP baseline  
307 (1); calibrated Noah-MP (2); difference between calibrated and baseline Noah-MP;  
308 VIC baseline (4); calibrated VIC (5); difference between calibrated and baseline VIC.





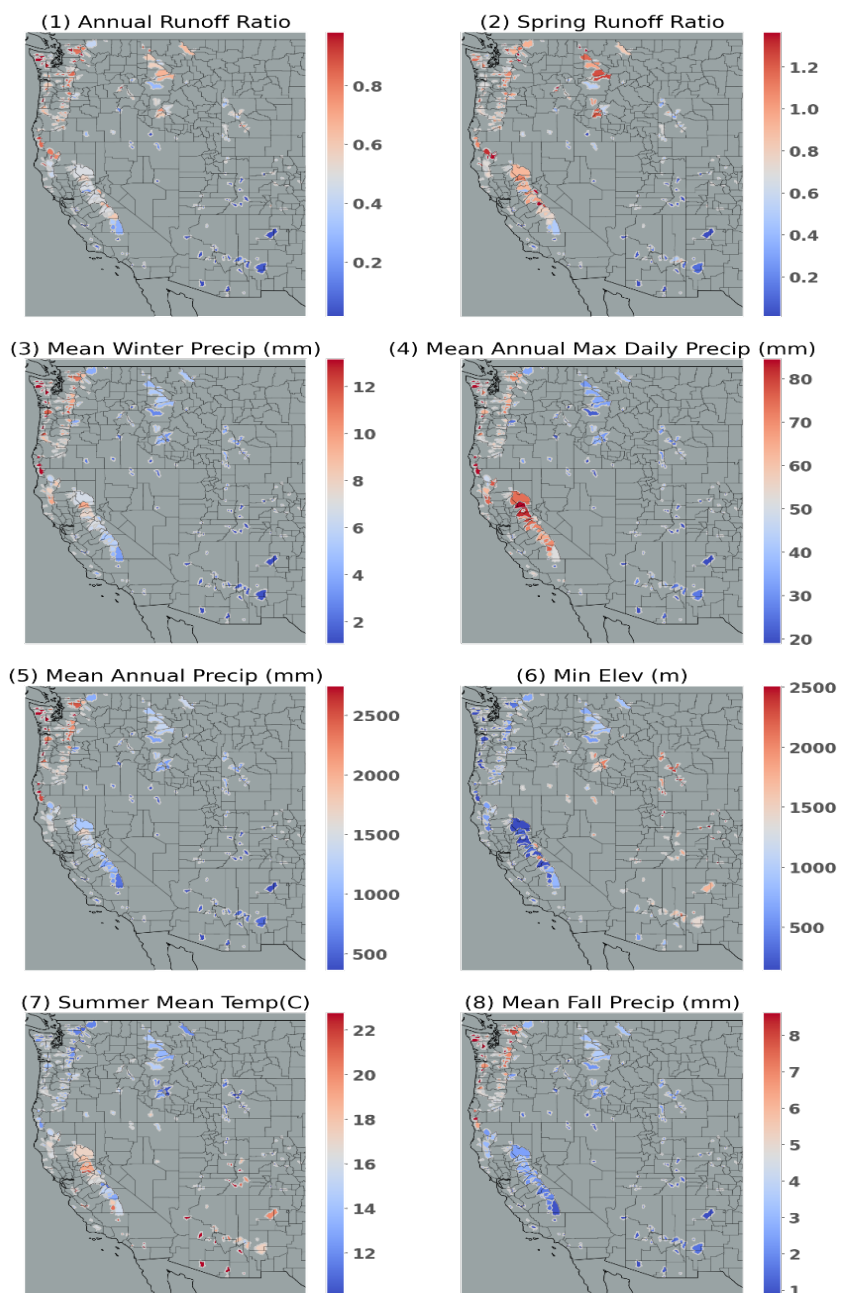
309

310 Figure 5. Scatterplots of VIC KGE in relation to significantly correlated  
311 characteristics. Each subplot indicates the corresponding Pearson correlation  
312 coefficients and the P-value.



313

314 Figure 6. Scatterplot of Noah-MP KGE in relation to significantly correlated  
315 characteristics. Each subplot indicates the corresponding Pearson correlation  
316 coefficients and the P-value.



317

318

319

320

Figure 7. Spatial distribution of characteristics that are statistically significantly correlated with KGE. Note that all characteristics are significantly correlated with VIC KGE whereas only (1)-(6) are significantly correlated with Noah-MP KGE.



#### 321        4.    Regionalization

322            Following the calibration process, we regionalized the parameters from gauged  
323 to ungauged basins based on a mathematical assessment of the spatial and physical  
324 proximity between the gauged and ungauged basins, following previous studies by  
325 Arsenault and Brissette (2014), and Razavi and Coulibaly (2017). We opted for this  
326 method over an alternate approach that first regionalizes the streamflow attributes  
327 (such as runoff depth, high flow indicators) and then standardizes the model  
328 throughout (as proposed by Castiglioni et al., 2010; Oubeidillah et al., 2014; and Yang  
329 et al 2017). The reason for our choice is our interest in actual streamflow time series  
330 rather than metrics. We carried out the regionalization after calibrating to specific  
331 streamflow gauges, ensuring high precision for these gauged basins and facilitating  
332 high-quality regionalization in ungauged basins. Specifically, we employed a donor-  
333 basin approach where an ungauged basin adopts calibrated parameters from its most  
334 similar gauged basin(s). This method has been applied in many studies including  
335 Arsenault and Brissette (2014); Poissant et al. (2017); Razavi and Coulibaly (2017);  
336 Gochis et al. 2019; Qi et al. (2021); and Bass et al (2023).

337            In the donor-basin method, an ungauged basin inherits its land surface  
338 parameters from the most similar gauged basin(s) (or the top 'x' most similar gauged  
339 basins). Here, we evaluated the similarity or proximity between gauged and ungauged  
340 basins based on the similarity index SI as defined and used by Burn and Boorman  
341 (1993) and Poissant et al. (2017):

$$342 \qquad SI = \sum_{i=1}^k \frac{|X_i^G - X_i^U|}{\Delta X_i} \qquad (1)$$

343            In this formula, k stands for the total number of features considered,  $X_i^G$  represents the  
344 ith feature of the gauged basin G,  $X_i^U$  is the ith feature of a specific ungauged basin,  
345 and  $\Delta X_i$  is the range of potential values for the ith feature, grounded in the data from



346 the gauged basins. This yields a unique value of SI for each gauged basin, contingent  
347 on the specific ungauged basin it is compared with. Typically, gauged basins that  
348 exhibit greater resemblance to the ungauged basin will have a smaller SI.

349 We assessed the donor-basin method's efficacy using a cross-validation approach,  
350 where each gauged basin was treated as ungauged one at a time. The pseudo-  
351 ungauged basin inherits its hydrological parameters from its three most similar  
352 gauged basins, determined by SI. The parameters inherited are a weighted average  
353 from the three donor basins. After testing one to five donor basins, we found that  
354 using three donors yielded the best results. Thus, every basin inherits parameters from  
355 the three most similar gauged basins in each simulation, offering a concise evaluation  
356 of the donor-basin method's regionalization performance.

357 We used 18 basin-specific features in the donor basin method, detailed in Table  
358 S1, calculated based on the forcings and parameters used in the study. For feature  
359 selection in the donor-basin method, we adopted an iterative approach. Each iteration  
360 added a single feature to the index, with the most beneficial feature (based on median  
361 KGE improvement) retained. This process was repeated until the median KGE no  
362 longer improved. Only basins with a KGE exceeding 0.3 were considered, following  
363 previous studies suggesting that inclusion of poorly performing basins can lower  
364 regionalization performance. We found that a KGE threshold of 0.3 resulted in a  
365 median performance improvement of 0.08 larger than did a KGE threshold of 0,  
366 hence it was chosen. After screening, 223 basins were utilized in VIC regionalization  
367 and 194 in Noah-MP regionalization.

368 We found five features generated the best regionalization performance for VIC  
369 (longitude centroid, latitude centroid, maximum elevation, fall mean precipitation,  
370 and fall mean temperature) and three features were best for Noah-MP (latitude  
371 centroid, longitude centroid, and drainage area) (see Figure 8). Among them, latitude



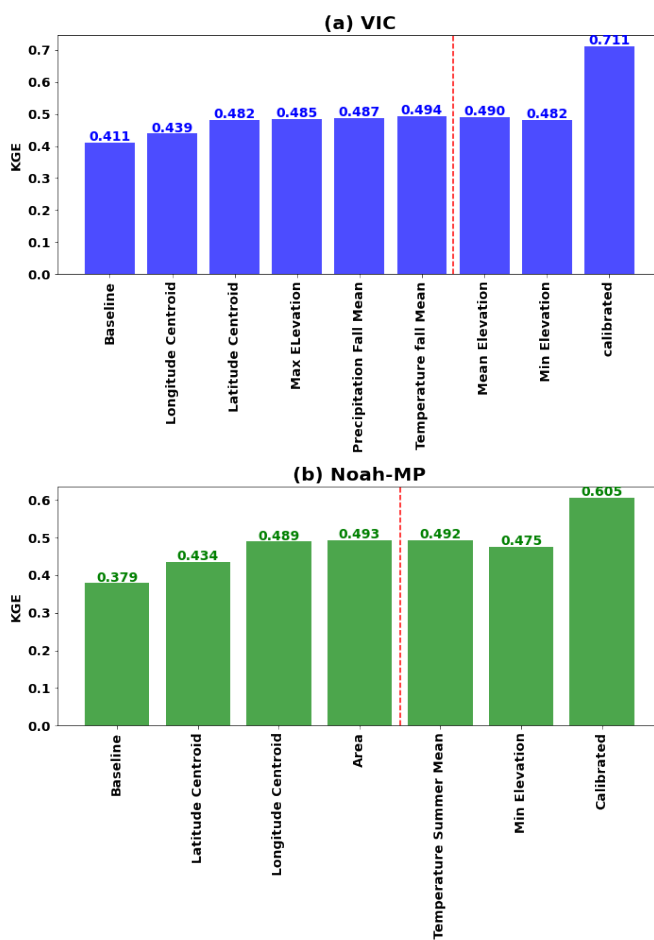
372 and longitude are the common features that contribute the most to regionalization  
373 when using the similarity index method. This suggests that geographical similarities  
374 are the most important factor in parameter information transfer from gauged to  
375 ungauged basins.

376       Upon evaluating the performance of baseline, calibrated, and regionalized  
377 simulations, the respective median daily KGEs for the VIC model were found to be  
378 0.41, 0.71, and 0.49. For the Noah-MP, these values were 0.38, 0.60, and 0.49 (refer  
379 to Figures 8 & 9). These metrics are for basins that have a calibrated KGE greater  
380 than 0.3 only, resulting in higher median KGEs than for all 263 basins (See Figure 3).  
381 The KGE distribution also improved overall. It's noteworthy that the regionalization  
382 improvement relative to baseline is higher for Noah-MP than for VIC. While VIC's  
383 baseline and calibrated KGE skill distribution outperforms Noah-MP's, the  
384 regionalized skills of Noah-MP and VIC are quite comparable. This observation might  
385 be attributable to the constraints of the regionalization setup and could warrant future  
386 investigation.

387       After optimizing the features and specific design of the donor-basin method,  
388 parameters were regionalized to 4816 ungauged USGS Hydrologic Unit Code (HUC)  
389 -10 basins across the WUS. HUCs are delineated and quality controlled by USGS  
390 using high-resolution DEMs. The final hydrologic parameters for both VIC and Noah-  
391 MP for all WUS HUC-10 basins are shown in Figures S1&2. The baseline HUC-10  
392 parameters are shown in Figures S3&4.

393

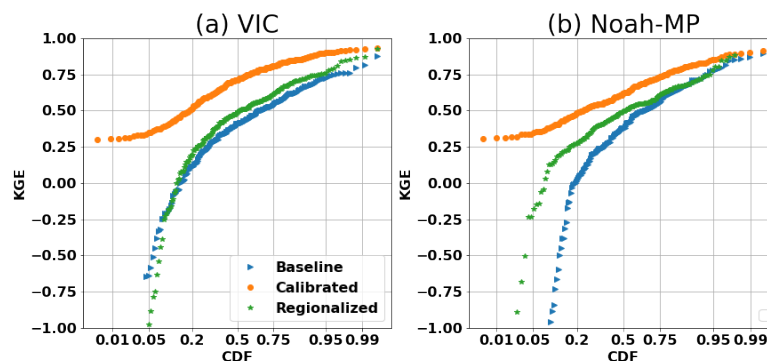
394



395

396 Figure 8. Best regionalization features for (a) VIC and (b) Noah-MP. The final  
397 regionalization to ungauged basins of the WUS incorporated all features up to the  
398 point marked by the red line since the addition of further features doesn't improve  
399 KGE.

400



401

402 Figure 9. CDF of daily KGE for (a) VIC and (b) Noah-MP, comparing baseline  
403 and calibrated runs across selected regionalized basins within the WUS.

## 404 5. Evaluation of high and low flow simulation skill

405 To understand the capabilities of the two models in reconstructing high and low  
406 streamflow, we assessed their performance across baseline, calibrated, and  
407 regionalized settings.

### 408 (a) Evaluation of high flow performance

409 We used the peaks-over-threshold (POT) method (Lang et al. 1999) to identify  
410 extreme streamflow events as in Su et al (2023) and Cao et al. (2019, 2020). We first  
411 applied the event independence criteria from USWRC (1982) to daily streamflow data  
412 to identify independent events. We set thresholds at each basin that resulted in 3  
413 extreme events per year on average. After selecting the flood events over the study  
414 period based on the observation, we sorted the floods based on the return period and  
415 then calculated the KGE of baseline, calibrated and regionalized floods. Figure 10  
416 displays the associated CDF plots. The median KGE for baseline floods in Noah-MP  
417 was 0.14, which rose to 0.37 post-calibration, and receded to 0.22 after  
418 regionalization. For VIC, the flood KGE started at 0.11, increased to 0.41 after  
419 calibration, and declined to 0.20 post-regionalization. As anticipated, these numbers

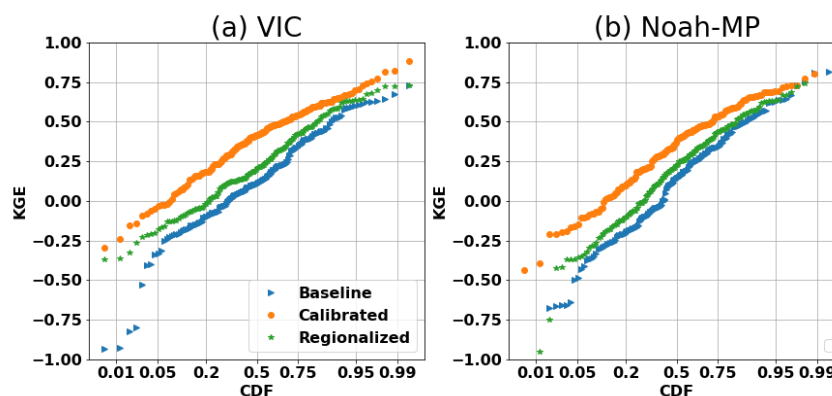




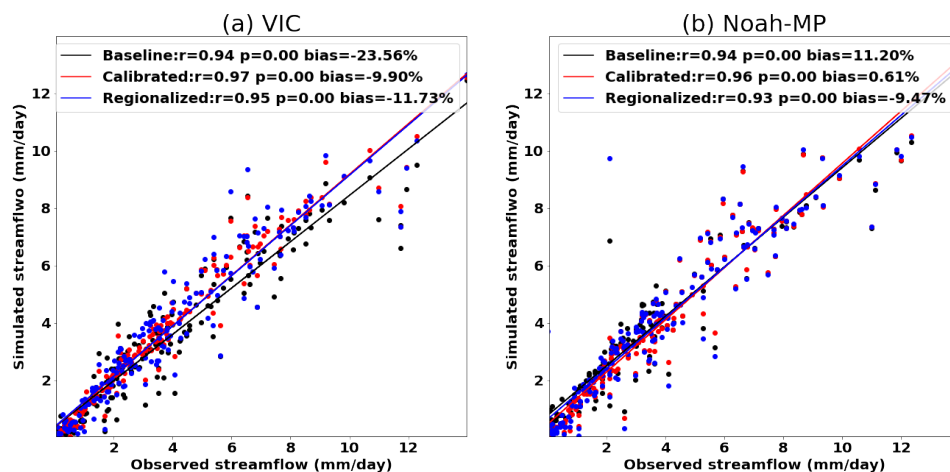
420 are lower than (all) daily streamflow skill due to our calibration target being daily  
421 streamflow. Still, flood competencies experienced considerable enhancement,  
422 surpassing the Noah-MP KGE benchmark of -0.41 found by Knoben et al. (2019).

#### 423 (b) Evaluation of low flow performance

424 To assess low flow performance, we utilized the 7q10 metric. This hydrological  
425 statistic, commonly adopted in water resources management and environmental  
426 engineering, is the lowest 7-day average flow that occurs (on average) once every 10  
427 years (EPA,2018). Scatterplots of 7q10 (Figure 11) showed high correlation between  
428 our model's simulated low flows and the observed data. Post-calibration, this  
429 alignment intensified. The VIC model tended to underestimate the low flows. After  
430 calibration, the median bias improved from -23.6% to -9.9%, and with  
431 regionalization, it was -11.7%. In contrast, Noah-MP began with an 11.20%  
432 overestimation in the baseline, improved to 0.61% post-calibration, and was -9.5%  
433 after regionalization. The outcomes underline the proficiency of both models for low  
434 flow prediction, exhibiting enhanced competencies post-calibration and commendable  
435 performance after regionalization.



436  
437 Figure 10. CDF of high flow KGE for (a) VIC and (b) Noah-MP, comparing  
438 baseline and calibrated runs across selected regionalized basins within the WUS.



439

440 Figure 11. Scatterplot of 7q10 low flows (the lowest 7-day average flow that  
441 occurs (on average) once every 10 years) for the baseline and calibrated and  
442 regionalized runs for (a) VIC model and (b) Noah-MP. The correlation coefficients, P-  
443 values and percentage bias are denoted in the upper section of the figures. The x axis  
444 is observed low flow and the y axis is simulated low flow.

## 445 6. Summary

446 Our objective was to produce parameter sets for VIC and Noah-MP over WUS  
447 that could be used in regional studies, and would result in better model performance  
448 than default or other “off the shelf” parameters. We identified preferred runoff  
449 generation options for Noah-MP (physics options are fixed in VIC) using a subset of  
450 our WUS basins (50 in total) for which we evaluated all four Noah-MP runoff  
451 generation options. Once we identified the optimal runoff generation options for  
452 Noah-MP, we identified (calibrated) parameters for both Noah-MP and VIC for each  
453 of our 263 basins across WUS using the most recently available 20-years of  
454 streamflow observations. Following calibration, the Noah-MP median KGE increased  
455 from 0.22 to 0.54, while the median VIC KGE rose from 0.37 to 0.70. VIC KGEs



456 were higher than Noah-MP's both before and after calibration across the 263 basins,  
457 possibly because the initial VIC parameters had the benefit of some previous  
458 calibration, albeit for much larger river basins across WUS (in the case of post-  
459 calibration KGE, it's unclear whether and how they might have been affected by the  
460 choice of initial parameters). Other possible cause of the differences could be  
461 inherent differences in streamflow simulation physics between the two models. We  
462 also conducted a test using the initial 10 years of data for calibration and the  
463 following 10 years for validation, and found results that were consistent with those we  
464 obtained using the entire 20 years for calibration.

465       Upon the selection of suitable parameterizations for Noah-MP and calibration of  
466 gauged basins for both VIC and Noah-MP, we extended the use of the calibrated  
467 parameters to ungauged basins across the WUS for both models. This extension was  
468 achieved through the donor-basin regionalization method, which allows ungauged  
469 basins to inherit parameters from gauged basins with similar hydroclimatic properties.  
470 We discovered that using a weighted combination of three similar basins yielded  
471 better regionalization results (in terms of KGE) compared to using the single most  
472 similar donor basin, as determined by a similarity index. Following regionalization,  
473 the median KGE for VIC rose from 0.41 to 0.49, and for Noah-MP it increased from  
474 0.38 to 0.49 over the selected basins. Interestingly, even though the pre-  
475 regionalization KGE for VIC was considerably higher than for Noah-MP, the post-  
476 regionalization values for the two models were nearly identical. Stated otherwise, the  
477 regionalization enhancement was considerably greater for Noah-MP than for VIC.  
478 We further evaluated high and low flow simulation skills and found the skill  
479 significantly improved after calibration for both VIC and Noah-MP and improvements  
480 remained after regionalization. Following calibration and regionalization, we  
481 developed gridded parameter sets for both models at 1/16° latitude-longitude



482 resolution for all 4816 HUC-10 basins across the WUS. These parameter sets should  
483 be useful for regional hydrologic and river hydrodynamic modeling studies over all or  
484 parts of the WUS domain. Improving the accuracy of the models' predictions should  
485 have benefits for water management across the region, and more and more generally  
486 for understanding the potential impacts of climate change across the region.  
487 Moreover, the methods and procedures we utilized are not restricted to our current  
488 research domain; they could be transferred readily to other geographic regions. In  
489 effect, our research contributes to both local and global efforts to understand and  
490 manage our critical hydrological systems better, demonstrating its broader relevance  
491 and utility.  
492



493 **Data Availability statement**

494 The Livneh (2013) forcings are available at

495 <http://livnehpublicstorage.colorado.edu:81/Livneh.2013.CONUS.Dataset/>. The

496 extended forcings used in this study are available at <ftp://livnehpublicstorage.>

497 [colorado.edu/public/sulu](http://colorado.edu/public/sulu). The results are available online at

498 <https://figshare.com/s/66fe8305bff516e80f6f>.

499

500 **Competing interests.** The contact author has declared that none of the authors has

501 any competing interests.



502 **References**

- 503 Adam, J.C. and Lettenmaier, D.P.: Adjustment of global gridded precipitation for  
504 systematic bias, *J. Geophys. Res.*, 108(D9), 1-14, doi:10.1029/2002JD002499,  
505 2003.
- 506 Adam, J.C., Clark, E.A. , Lettenmaier, D.P. and Wood, E.F.: Correction of Global  
507 Precipitation Products for Orographic Effects, *J. Clim.*, 19(1), 15-38, doi:  
508 10.1175/JCLI3604.1, 2006.
- 509 Anghileri, D., Voisin, N., Castelletti, A., Pianosi, F. , Nijssen, B. and Lettenmaier,  
510 D.P.: Value of Long-Term Streamflow Forecasts to Reservoir Operations for  
511 Water Supply in Snow-Dominated River Catchments. *Water Resources Research*  
512 52: 4209–25, 2016.
- 513 Arsenault, R., and Brissette, F. P.: Continuous streamflow prediction in ungauged  
514 basins: The effects of equifinality and parameter set selection on uncertainty in  
515 regionalization approaches. *Water Resour. Res.*, 50, 6135–6153, [https://doi.org/](https://doi.org/10.1002/2013WR014898)  
516 10.1002/2013WR014898, 2014.
- 517 Bass, B., Rahimi, S., Goldenson, N., Hall, A., Norris, J. and Lebow, Z.J.: Achieving  
518 Realistic Runoff in the Western United States with a Land Surface Model Forced  
519 by Dynamically Downscaled Meteorology. *Journal of Hydrometeorology*, 24(2),  
520 269-283, 2023.
- 521 Bennett, A. R., Hamman, J. J. and Nijssen, B.: MetSim: A Python package for  
522 estimation and disaggregation of meteorological data. *J. Open Source Software*,  
523 5, 2042, <https://doi.org/10.21105/joss.02042>, 2020.
- 524 Beven, K.: Changing ideas in hydrology-the case of physically-based models. *Journal*  
525 *of Hydrology*, 105(1-2), 157–172. [https://doi.org/10.1016/0022-1694\(89\)90101-](https://doi.org/10.1016/0022-1694(89)90101-7)  
526 7, 1989.



- 527 Bohn, T. J., Livneh, B., Oyler, J. W., Running, S. W., Nijssen, B. and Lettenmaier, D.  
528 P.: Global evaluation of MTCLIM and related algorithms for forcing of  
529 ecological and hydrological models. *Agric. For. Meteorol.*, 176, 38–49,  
530 <https://doi.org/10.1016/j.agrformet.2013.03.003>, 2013.
- 531 Boucher, M.-A., and Ramos, M.-H.: Ensemble Streamflow Forecasts for Hydropower  
532 Systems. In *Handbook of Hydrometeorological Ensemble Forecasting*, edited by  
533 Q. Duan, F. Pappenberger, J. Thielen, A. Wood, H.L. Cloke, and J.C. Schaake, 1–  
534 19. Berlin Heidelberg: Springer, 2018.
- 535 Burn, D. H., and Boorman, D. B.: Estimation of hydrological parameters at ungauged  
536 catchments. *J. Hydrol.*, 143,429454, [https://doi.org/10.1016/0022-](https://doi.org/10.1016/0022-1694(93)90203-L)  
537 [1694\(93\)90203-L](https://doi.org/10.1016/0022-1694(93)90203-L), 1993.
- 538 Cai, X., Yang, Z.-L. , David, C. H., Niu, G.-Y. and Rodell, M.: Hydrological  
539 evaluation of the Noah-MP land surface model for the Mississippi River Basin. *J.*  
540 *Geophys. Res. Atmos.*, 119, 23–38, <https://doi.org/10.1002/2013JD020792>,  
541 2014.
- 542 California Department of Water Resources: California data exchange center: Daily  
543 full natural flow for December 2022. California Department of Water Resources,  
544 accessed 1 October 2021, [https://cdec.water.ca.gov/reportapp/javareports?name=](https://cdec.water.ca.gov/reportapp/javareports?name=FNF)  
545 [FNF](https://cdec.water.ca.gov/reportapp/javareports?name=FNF), 2021.
- 546 Cao, Q., Mehran, A. , Ralph, F. M. and Lettenmaier, D. P.: The role of hydrological  
547 initial conditions on atmospheric river floods in the Russian River basin. *J.*  
548 *Hydrometeorol.*, 20, 16671686, <https://doi.org/10.1175/JHM-D-19-0030.1>, 2019.
- 549 Cao, Q., Gershunov, A., Shulgina, T., Ralph, F. M. , Sun, N. and Lettenmaier, D. P.:  
550 Floods due to atmospheric rivers along the U.S. West Coast: The role of  
551 antecedent soil moisture in a warming climate. *J. Hydrometeorol.*, 21, 1827–1845,  
552 [https:// doi.org/10.1175/JHM-D-19-0242.1](https://doi.org/10.1175/JHM-D-19-0242.1), 2020.



- 553 Castiglioni, S., Lombardi, L., Toth, E., Castellarin, A. and Montanari, A.: Calibration  
554 of rainfall-runoff models in ungauged basins: A regional maximum likelihood  
555 approach. *Advances in Water Resources*, 33(10), 1235–1242.  
556 <https://doi.org/10.1016/j.advwatres.2010.04.009>, 2010.
- 557 Chen, F., and Dudhia, J.: Coupling an advanced land surface–hydrology model with  
558 the Penn State–NCAR MM5 modeling system. Part I: Model implementation  
559 and sensitivity. *Mon. Wea. Rev.*, 129, 569–585, [https://doi.org/10.1175/1520-0493\(2001\)129<0569:CAALSH>2.0.CO;2](https://doi.org/10.1175/1520-0493(2001)129<0569:CAALSH>2.0.CO;2), 2001.
- 561 Chen, F., and Coauthors: Modeling of land-surface evaporation by four schemes and  
562 comparison with FIFE observations. *J. Geophys. Res.*, 101, 7251–7268,  
563 <https://doi.org/10.1029/95JD02165>, 1996.
- 564 Cosby, B.J., Hornberger, G.M., Clapp, R.B. and Ginn, T.: A statistical exploration of  
565 the relationships of soil moisture characteristics to the physical properties of  
566 soils. *Water resources research*, 20(6), 682–690, 1984.
- 567 Dickinson, R. E., Henderson-Sellers, A. & Kennedy, P. J.: Biosphere–Atmosphere  
568 Transfer Scheme (BATS) version 1e as coupled to the NCAR Community  
569 Climate Model. NCAR Tech. Note TN383+STR, NCAR, 1993.
- 570 Duan, Q., Sorooshian, S. and Gupta, V. : Effective and efficient global optimization  
571 for conceptual rainfall-runoff models. *Water Resour. Res.*, 28, 1015–1031,  
572 <https://doi.org/10.1029/91WR02985>, 1992.
- 573 Environmental Protection Agency (EPA) Office of Water: Low Flow Statistics Tools:  
574 A How-To Handbook for NPDES Permit Writers. EPA-833-B-18-001, 2018.
- 575 Falcone, J.: GAGES-II: Geospatial attributes of gages for evaluating streamflow. U.S.  
576 Geological Survey, accessed 1 April 2021,  
577 [https://water.usgs.gov/GIS/metadata/usgswrd/XML/gagesII\\_Sept2011.xml](https://water.usgs.gov/GIS/metadata/usgswrd/XML/gagesII_Sept2011.xml),  
578 2011.





- 579 Federal Institute of Hydrology: “SOSRHINE.”  
580 [http://sosrhine.euporias.eu/en/sosrhine\\_overview](http://sosrhine.euporias.eu/en/sosrhine_overview), 2020.
- 581 Fisher, R.A. and Koven, C.D.: Perspectives on the future of land surface models and  
582 the challenges of representing complex terrestrial systems. *Journal of Advances*  
583 *in Modeling Earth Systems*, 12(4), p.e2018MS001453, 2020.
- 584 Gochis, D. and Coauthors: Overview of National Water Model Calibration: General  
585 strategy and optimization. National Center for Atmospheric Research, accessed 1  
586 January 2023, 30 pp.,  
587 [https://ral.ucar.edu/sites/default/files/public/9\\_RafieeiNasab\\_CalibOverview\\_CU](https://ral.ucar.edu/sites/default/files/public/9_RafieeiNasab_CalibOverview_CU)  
588 [AHSI\\_Fall019\\_0.pdf](https://ral.ucar.edu/sites/default/files/public/9_RafieeiNasab_CalibOverview_CU), 2019.
- 589 Gong, W., Duan, Q., Li, J., Wang, C., Di, Z., Dai, Y., et al.: Multi-objective parameter  
590 optimization of common land model using adaptive surrogate modeling.  
591 *Hydrology and Earth System Sciences*, 19(5), 2409–2425.  
592 <https://doi.org/10.5194/hess-19-2409-2015>, 2015.
- 593 Gou, J., Miao, C., Duan, Q., Tang, Q., Di, Z., Liao, W., Wu, J. and Zhou, R.:  
594 Sensitivity analysis-based automatic parameter calibration of the VIC model for  
595 streamflow simulations over China. *Water Resources Research*, 56(1),  
596 e2019WR025968, 2020.
- 597 Gupta, H. V., et al.: Decomposition of the mean squared error and NSE performance  
598 criteria: Implications for improving hydrological modelling. *Journal of*  
599 *Hydrology*, 377, 80-91,2009.
- 600 Holtzman, N.M., Pavelsky, T.M., Cohen, J.S., Wrzesien, M.L. and Herman, J.D.:  
601 Tailoring WRF and Noah-MP to improve process representation of Sierra  
602 Nevada runoff: Diagnostic evaluation and applications. *Journal of Advances in*  
603 *Modeling Earth Systems*, 12(3), p.e2019MS001832, , 2020.
- 604 Hussein, A.: Process-based calibration of WRF-hydro model in unregulated



605 mountainous basin in Central Arizona. M.S. thesis, Ira A. Fulton Schools of  
606 Engineering, Arizona State University, 110 pp.,  
607 [https://keep.lib.asu.edu/\\_flysystem/fedora/  
608 c7/224690/Hussein\\_asu\\_0010N\\_19985.pdf](https://keep.lib.asu.edu/_flysystem/fedora/c7/224690/Hussein_asu_0010N_19985.pdf), 2020.

609 Kimball, J. S., Running, S. W. and Nemani, R. R.: An improved method for  
610 estimating surface humidity from daily minimum temperature. *Agric. For.  
611 Meteor.*, 85, 87–98, [https:// doi.org/10.1016/S0168-1923\(96\)02366-0](https://doi.org/10.1016/S0168-1923(96)02366-0), 1997.

612 Lahmers, T.M., et al.: Evaluation of NOAA national water model parameter  
613 calibration in semiarid environments prone to channel infiltration. *Journal of  
614 Hydrometeorology*, 22(11), 2939-2969, 2021.

615 Li, D., Lettenmaier, D. P., Margulis, S. A. and Andreadis, K.: Theroleofrain-on-  
616 snowinflooding over the conterminous United States. *Water Resour. Res.*, 55,  
617 8492–8513, <https://doi.org/10.1029/2019WR024950>, 2019.

618 Liang, X., Lettenmaier, D. P. , Wood, E. F. and Burges S. J. : A simple hydrologically  
619 based model of land surface water and energy fluxes for general circulation  
620 models, *J. Geophys. Res.*, 99(D7), 14415–14428, doi:10.1029/94JD00483, 1994.

621 Livneh B, Rosenberg, E.A. , Lin, C. , Nijssen, B. , Mishra, V. , Andreadis, K. ,  
622 Maurer, E.P. and Lettenmaier, D.P.: A long-term hydrologically based data set of  
623 land surface fluxes and states for the conterminous United States: Updates and  
624 extensions, *Journal of Climate*, doi:10.1175/JCLI-D-12-00508.1, 2013.

625 Maidment, D.R.: Conceptual Framework for the National Flood Interoperability  
626 Experiment. *Journal of the American Water Resources Association* 53: 245–57,  
627 2017.

628 Mascaro, G., Hussein, A., Dugger, A. and Gochis, D.J.: Process-based calibration of  
629 WRF-Hydro in a mountainous basin in southwestern US. *Journal of the  
630 American Water Resources Association*, 59(1), 49-70, 2023.



- 631 Mendoza, P.A., Clark, M.P., Mizukami, N., Newman, A.J., Barlage, M., Gutmann,  
632 E.D., Rasmussen, R.M., Rajagopalan, B., Brekke, L.D. and Arnold, J.R.: Effects  
633 of hydrologic model choice and calibration on the portrayal of climate change  
634 impacts. *Journal of Hydrometeorology*, 16(2), 762-780, 2015.
- 635 Miller, D.A. and White, R.A.: A conterminous United States multilayer soil  
636 characteristics dataset for regional climate and hydrology modeling. *Earth  
637 interactions*, 2(2), pp.1-26, 1998.
- 638 Naeini, M.R., Analui, B., Gupta, H.V., Duan, Q. and Sorooshian, S.. Three decades of  
639 the Shuffled Complex Evolution (SCE-UA) optimization algorithm: Review and  
640 applications. *Scientia Iranica*, 26(4), pp.2015-2031, 2019.
- 641 Niu, G.-Y., Yang, Z.-L. , Dickinson, R. E. , Gulden, L. E. and Su, H.: Development of  
642 a simple groundwater model for use in climate models and evaluation with  
643 gravity recovery and climate experiment data. *J. Geophys. Res.*, 112, D07103,  
644 <https://doi.org/10.1029/2006JD007522>, 2007.
- 645 Niu, G. Y., Yang, Z. L., Dickinson, R. E., & Gulden, L. E.: A simple TOPMODEL-  
646 based runoff parameterization (SIMTOP) for use in global climate models.  
647 *Journal of Geophysical Research: Atmospheres*, 110(D21), 2005.
- 648 Niu, G.-Y., and Coauthors: The community Noah land surface model with  
649 multiparameterization options (Noah-MP): 1. Model description and evaluation  
650 with local-scale measurements. *J. Geophys. Res.*, 116, D12109,  
651 <https://doi.org/10.1029/2010JD015139>, 2011.
- 652 NOAA (National Oceanic and Atmospheric Administration): National Water Model:  
653 Improving NOAA's Water Prediction Services, 2016.
- 654 Oubeidillah, A. A., Kao, S.-C., Ashfaq, M. , Naz, B. S. and Tootle, G.: A large-scale,  
655 high-resolution hydrological model parameter data set for climate change impact  
656 assessment for the conterminous US. *Hydrology and Earth System Sciences*,



- 657 18(1), 67–84. [https://doi.org/ 10.5194/hess-18-67-2014](https://doi.org/10.5194/hess-18-67-2014), 2014.
- 658 Prata, A.J.: A new long-wave formula for estimating downward clear-sky radiation at  
659 the surface. Quarterly Journal of the Royal Meteorological Society, 122(533),  
660 1127-1151, 1996.
- 661 Poissant, D., Arsenault, A. and Brissette, F. : Impact of parameter set dimensionality  
662 and calibration procedures on streamflow prediction at ungauged catchments. J.  
663 Hydrol. Reg. Stud., 12,220–237, <https://doi.org/10.1016/j.ejrh.2017.05.005>,  
664 2017.
- 665 Qi, W.Y., Chen, J. , Li, L. , Xu, C.-Y. , Xiang, Y.-h. , Zhang, S.-B. and Wang, H.-M.:  
666 Impact of the number of donor catchments and the efficiency threshold on  
667 regionalization performance of hydrological models. J. Hydrol., 601, 126680,  
668 <https://doi.org/10.1016/j.jhydrol.2021.126680>, 2021.
- 669 Raff, D., Brekke, L. , Werner, K. , Wood, A. and White. K.: Short-Term Water  
670 Management Decisions: User Needs for Improved Climate, Weather, and  
671 Hydrologic Information. U.S. Bureau of Reclamation.  
672 <https://www.usbr.gov/research/st/roadmaps/WaterSupply.pdf>, 2013.
- 673 Razavi, T., and Coulibaly, P.: An evaluation of regionalization and watershed  
674 classification schemes for continuous daily streamflow prediction in ungauged  
675 watersheds. Can. Water Resour. J., 42,2–20,  
676 <https://doi.org/10.1080/07011784.2016.1184590>, 2017.
- 677 Schaake, J. C., Koren, V. I., Duan, Q.-Y., Mitchell, K., & Chen, F.: Simple water  
678 balance model for estimating runoff at different spatial and temporal scales.  
679 Journal of Geophysical Research, 101(D3), 7461–7475.  
680 <https://doi.org/10.1029/95JD02892>, 1996.
- 681 Schaperow J.R, Li, D., Margulis, S.A., Lettenmaier D.P. :A near-global, high  
682 resolution land surface parameter dataset for the variable infiltration capacity



- 683 model. Scientific Data. Aug 11;8(1):216, 2021.
- 684 Sharma, P. and Machiwal, D.: Streamflow forecasting: overview of advances in data-  
685 driven techniques. Advances in Streamflow Forecasting,1-50.  
686 <https://doi.org/10.1016/B978-0-12-820673-7.00013-5>, 2021
- 687 Shi, X., Wood, A.W. and Lettenmaier, D.P. : How essential is hydrologic model  
688 calibration to seasonal streamflow forecasting? Journal of Hydrometeorology,  
689 9(6), 1350-1363, 2008.
- 690 Sofokleous, I., Bruggeman, A., Camera, C. and Eliades, M.: Grid-based calibration of  
691 the WRF-Hydro with Noah-MP model with improved groundwater and  
692 transpiration process equations. Journal of Hydrology, 617, 128991 , 2023
- 693 Su, L., Cao, Q. , Xiao, M., Mocko, D. M., Barlage, M. , Li, D. , Peters-Lidard, C. D.  
694 and Lettenmaier, D. P.: Drought variability over the conterminous United States  
695 for the past century. J. Hydrometeor., 22, 1153–1168,  
696 <https://doi.org/10.1175/JHM-D-20-0158.1>, 2021.
- 697 Su, L., Cao, Q. , Shukla, S., Pan, M. and Lettenmaier, D.P.: Evaluation of Subseasonal  
698 Drought Forecast Skill over the Coastal Western United States. Journal of  
699 Hydrometeorology, 24(4), 709-726, 2023.
- 700 Tangdamrongsub, N.: Comparative Analysis of Global Terrestrial Water Storage  
701 Simulations: Assessing CABLE, Noah-MP, PCR-GLOBWB, and GLDAS  
702 Performances during the GRACE and GRACE-FO Era. Water, 15(13), p.2456,  
703 2023.
- 704 Thornton, P. E., and Running, S. W.: An improved algorithm for estimating incident  
705 daily solar radiation from measurements of temperature, humidity, and  
706 precipitation. Agric. For. Meteor., 93, 211–228, [https://doi.org/10.1016/S0168-](https://doi.org/10.1016/S0168-1923(98)00126-9)  
707 1923(98) 00126-9, 1999.
- 708 Tolson, B. A., and Shoemaker, C. A.: Dynamically dimensioned search algorithm for



709 computationally efficient watershed model calibration. *Water Resour. Res.*, 43,  
710 W01413, <https://doi.org/10.1029/2005WR004723>, 2007.

711 Troy, T. J., Wood, E. F. and Sheffield, J.: An efficient calibration method for  
712 continental-scale land surface modeling. *Water Resources Research*, 44,  
713 W09411. <https://doi.org/10.1029/2007WR006513>, 2008

714 [USWRC: Guidelines for determining flood flow frequency. Bulletin 17B of the](#)  
715 [Hydrology Subcommittee, 183 pp., https://](#)  
716 [water.usgs.gov/osw/bulletin17b/dl\\_flow.pdf](https://water.usgs.gov/osw/bulletin17b/dl_flow.pdf), 1982.

717 [Yang, Y., Pan, M., Beck, H.E., Fisher, C.K., Beighley, R.E., Kao, S.C., Hong, Y. and](#)  
718 [Wood, E.F.: In quest of calibration density and consistency in hydrologic](#)  
719 [modeling: Distributed parameter calibration against streamflow characteristics.](#)  
720 [Water Resources Research, 55\(9\), 7784-7803, 2019.](#)

721 Yang, Z.-L., and Dickinson R. E. : Description of the BiosphereAtmosphere Transfer  
722 Scheme (BATS) for the soil moisture workshop and evaluation of its  
723 performance, *Global Planet. Change*, 13, 117–134, doi:10.1016/0921-  
724 8181(95)00041-0, 1996.

725 Zheng, H., Yang, Z.-L., Lin, P., Wei, J., Wu, W.-Y., Li, L., Zhao, L. and Wang, S.:  
726 On the sensitivity of the precipitation partitioning into evapotranspiration and  
727 runoff in land surface parameterizations. *Water Resour. Res.*, 55, 95–111,  
728 <https://doi.org/10.1029/2017WR022236>, 2019.